Paper-Based Bistable Origami Gripper to Make Quadcopters Multi-Functional

Shuta Okamoto, Yuki Fukatsu, Chinthaka Premachandra, *Senior Member, IEEE*, and Hiroki Shigemune, *Member, IEEE*

***Abstract*—Quadcopters have many promising applications in transportation, agriculture, construction, and environmental monitoring. For further utilization, researches on attaching grasping function devices such as manipulators and grippers to quadcopters are gaining attention. Device mounting significantly impacts flight due to weight and center-of-gravity shifts. We developed a self-folded origami gripper (SOG) based on paper self-folding technology. The SOG consists of a bistable structure and a multilayer cylindrical structure. The origami structure is created by self-folding technology using ink-jet printing, which gives the paper elastic hinges and rigidity. The optimal parameters for designing the grasping function of the SOG were identified to improve the grasping performance. The SOG itself weighs only 5 g, yet it demonstrated grasping force equivalent to holding a 130 g object in the grasping force experiment. Eventually, the developed SOG was mounted on a quadcopter, and flight-grasping experiments were successfully conducted. The developed SOG is made entirely of paper, a biodegradable material. When the SOG falls to the ground due to an accident or deterioration, it is expected to be used as a green grasping device that returns to the soil and does not destroy the environment.**

***Index Terms*—Soft robot materials and design, grasping, bistable mechanism, origami, paper mechatronics.**

I. Introduction

In RECENT years, the development of quadcopters for industrial applications has been active. For example, the advantages of unmanned operation to reduce labor costs, environmental monitoring through aerial photography, and access to difficult-to-access areas have led to consideration of applications in transportation, agriculture, construction, surveying, and disaster management. For further utilization, research is emerging to attach grasping devices such as manipulators and grippers.

Manuscript received 15 September 2023; accepted 22 February 2024. Date of publication 13 March 2024; date of current version 4 April 2024. This letter was recommended for publication by Associate Editor H. Sato and Editor C. Laschi upon evaluation of the reviewers' comments. This work was supported in part by the JSPS KAKENHI under Grant JP22K14226, in part by New Energy and Industrial Technology Development Organization (NEDO) under Project JPNP20004, and in part by the Fuji Seal Foundation and International Research Center for Green Electronics at Shibaura Institute of Technology. *(Corresponding author: Hiroki Shigemune.)*

Shuta Okamoto and Yuki Fukatsu are with the Department of Electrical Engineering, Shibaura Institute of Technology, Tokyo 135-8548, Japan.

Chinthaka Premachandra is with the Department of Electronic Engineering, Shibaura Institute of Technology, Tokyo 135-8548, Japan.

Hiroki Shigemune is with the Department of Electrical Engineering, Shibaura Institute of Technology, Tokyo 135-8548, Japan, and also with the International Research Center for Green Electronics, Shibaura Institute of Technology, Tokyo 135-8548, Japan (e-mail: hshige@shibaura-it.ac.jp).

This letter has supplementary downloadable material available at https://doi.org/10.1109/LRA.2024.3376972, provided by the authors.

Digital Object Identifier 10.1109/LRA.2024.3376972

Grasping function devices have been studied using various materials and means [1]. For example, pneumatic grippers [2], electroadhesive soft grippers [3], and kirigami grippers [4]. These developments bring multifunctionality to quadcopters. However, the weight and center of gravity, which change with the loading of grasping and control devices, are problems. When the lift force is smaller than the weight of the devices, takeoff becomes not possible. Shifts in the center of gravity affect flight and make it difficult to achieve the desired operation. For these reasons, grasping devices are being developed to reduce weight, size, and simplify control [5], [6], [7], [8], [9].

Origami technology reproduces complex three-dimensional structures through the simple topology of folding two-dimensional sheet material. By calculating the fold pattern, the structure has various mechanical properties such as deplorability, foldability, and flexibility [10], [11], [12], [13], [14]. The origami structure has a high affinity for mounting on a quadcopter because it is hollow, making it lightweight and rigid. From these advantages, researches have utilized origami structures in lightweight robotic arms [15], protectors [16], sensor-attached devices [6], and foldable arms [17]. However, the more functional the origami structures become, the more complex the fabrication process becomes. To overcome the disadvantages, self-folding technologies that fabricate origami structures by automatically folding sheet materials have been studied [18], [19], [20].

Conventional grasping devices for mounting to the quadcopter require the integration of a power supply and sensors. To solve this problem, grasping devices that achieve a new means of grasping were developed [6], [8], [9]. Integrating the bistable structure into the grasping mechanism, a simple control that allowed grasping only by contact with the object was conducted [6], [9]. However, to integrate the bistable structure, it was necessary to combine multiple rigid and flexible materials. This made the entire system more complex and increases the risk of malfunction. Besides, the use of environmentally harmful materials such as plastic and resin materials is undesirable considering their use in a wide variety of environments, such as crop harvesting in large agricultural areas and environmental surveys in vast forests. Therefore, it is necessary to introduce environmentally friendly green materials.

This study proposes a simple-to-control and lightweight soft gripper based on origami technology. The developed gripper is called the Self-folded Origami Gripper (SOG), which consists of a bistable mechanism and a multilayer cylindrical structure. SOG is fabricated from biodegradable material, which is a paper. SOG uses the bistable mechanism to switch between opening and closing. This allows the object to be grasped passively only by contact. There is no requirement to control the timing or force

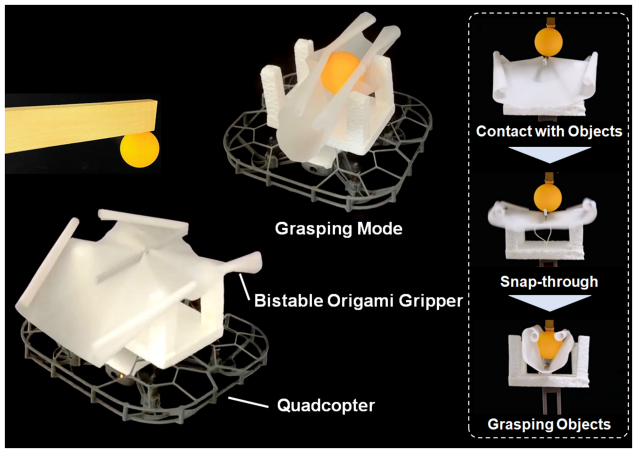

Fig. 1. Self-folded origami gripper on a quadcopter. The object can be grasped by applying force to its target point using a mechanism composed exclusively of paper materials.

of the grasp, and no control circuit is required, thus achieving compactness of the whole system. SOG inherits the lightweight property of paper, allowing it to be mounted on a quadcopter and fly stably. In addition, the multilayer cylindrical structure was developed and adopted for the finger part. Rigidity is increased by folding the sheet into a multilayer cylindrical shape. Our proposed analytical solution can calculate the theoretical value of the second area moment for the multilayer cylindrical structure. Then, it was confirmed that there is a correlation between the stiffness of the finger and performance of the gripper, and force to grasp a 130 g object was successfully demonstrated in the grasping experiment. Finally, the developed gripper was equipped on a quadcopter, and achieved to grasp the object while flying operation.

II. Self-Folded Origami Gripper

A. Design Concept

The gripper structure is created by self-folding technology using inkjet printing [21]. The origami structure is formed autonomously by a physicochemical reaction between the solution ejected from the inkjet printer and the paper. Fig. 2 shows the characteristic mechanical property of the self-folded paper. Fig. 2(a) shows that the folding angle can be controlled by changing the printing line width. When the printing line width is p_w, the paper bends with a constant curvature ρ, therefore the bending angle $\theta = \rho p_w$. Moreover, as shown in Fig. 2(b), the hinge acquires elastic memory characteristics. When an external force is removed, the structure returns to its original shape. Stretchability that automatically restores the initial state can be realized. The elastic memory feature is essential to provide grasping ability to the SOG.

Fig. 3 shows the fabrication process. First, the paper is cut using a cutting plotter (Silhouette CAMEO4 PLUS, Graphtec). Next, the cut paper is printed by an inkjet printer (DCP-J540N, brother). Then, the paper automatically forms a valley fold along the print line. The method of preparation follows previous our studies and uses equivalent materials [22]. Generally, a power supply or additional components are required to drive actuators for self-folding. However, the SOG employes reaction-based

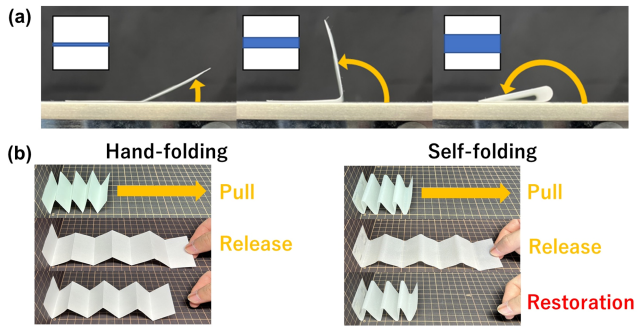

Fig. 2. Characteristic Mechanical property of the self-folded paper. (a) Control of folding angle through variation of printing line width. (b) Elastic memory characteristics to hinge sections of the self-folded paper.

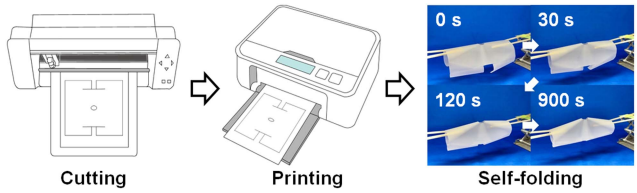

Fig. 3. Fabrication process of a self-folded origami gripper (SOG). After printing both sides of the cut paper, the paper self-folds along the printing lines, and forms the SOG.

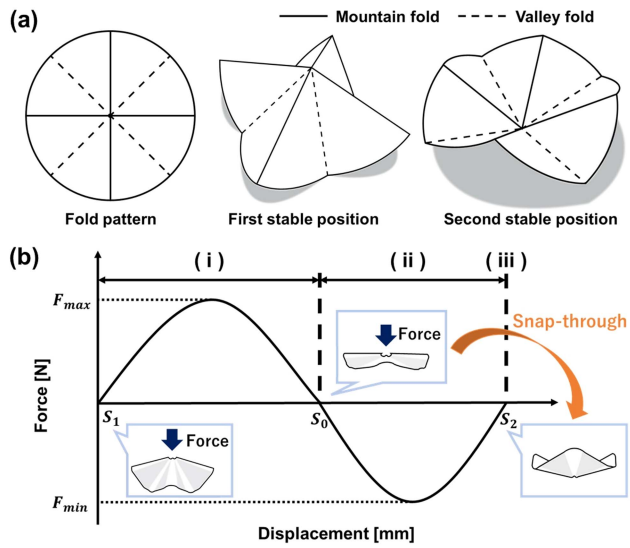

Fig. 4. Mechanism of bistable structure. (a) Water bomb structure. Bistable structures can be imparted to a sheet by alternately folding it in mountain and valley folds in a circular manner. (b) Principle.

self-folding technology, therefore it can be fabricated from a paper sheet without adding new components. The SOG only consists with the paper material and retains the characteristics of a green device with low environmental impact.

B. Bistable Structure

We applied the water bomb structure as the bistable mechanism [23], [24]. Fig. 4(a) shows a schematic diagram of the origami water bomb structure. The water bomb structure uses a

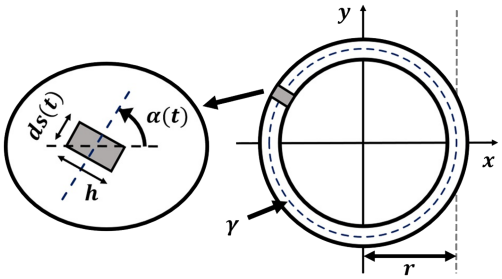

Fig. 5. Analysis on second area moment of hollow circular structure. Integrating the microelements along the circular structure allows the derivation of the second area moment.

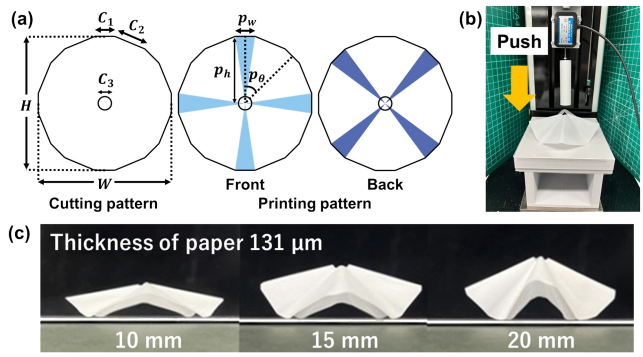

Fig. 6. Design and experimental setup of bistable structure. (a) Cutting and printing patterns. (b) Compression test. (c) Prototype.

simple fold pattern to impart bistable behavior and spring characteristics for a sheet material. Fig. 4(b) shows the mechanism of the bistable structure. The bistable structure has two stable states (S_1, S_2), and does not require a continuous input of force to maintain these states; external forces switch S_1 and S_2. When a force greater than F_{max} is applied downward to the top of a mountain at S_1 (Fig. 4(b)(i)), snap-through occurs after passing through S_0 (Fig. 4(b)(ii)), and then it shifts to S_2 (Fig. 4(b)(iii)). When a force of more than $|F_{min}|$ is applied upward to the valley's top, it switches from S_2 to S_1 through S_0, which follows the opposite direction to the above process.

Comparing with the hand-folded bistable structure, the self-folded bistable structure showed stable mechanical property in the preliminary experiment. The elastic memory property of the self-folded paper provides high grasping and repetition performance for the gripper.

C. Multilayer Cylindrical Structure

The rigidity of the fingers dominates the weight of the graspable object. The paper was self-folded into a cylindrical shape to create the multilayer cylindrical structure. The circularity improves the second area moment and increases rigidity. The open origami structures are known to be structurally strengthened by stacking [25].

To estimate the stiffness of the multilayer cylindrical structure, we derive the analytical solution for second area moment of the hollow circular cross-section as shown in Fig. 5. γ is the midline of the circular curve, r is the radius, and h is the thickness. The midline curve γ is expressed by

$$\gamma = [x\,(t)\,,\ y\,(t)] = \ [r\cos\,(\pi t)\,,\ r sin\,(\pi t)] \tag{1}$$

From the formula for the second area moment of an inclined rectangle cross-sections and the parallel axis theorem, the infinitesimal second area moment dI along curves follows.

$$\begin{aligned} dI \ &= \frac{h\ ds}{12}\ \left(h^2\cos^2\,(\alpha) + ds^2\sin^2\,(\alpha)\right) + y(t)^2 h\ ds \\ &\cong \frac{h^3}{12}\cos^2\,(\alpha)\,ds + y(t)^2 h\ ds \end{aligned} \tag{2}$$

The relationships in (3) and (4) hold here. Therefore, integrating (2) along the midline curve γ yields the analytical solution for the second area moment of the cross-section.

$$\cos\,(\alpha\,(t)) \ = \frac{x'\,(t)}{\sqrt{x'(t)^2 + y'(t)^2}} \tag{3}$$

$$ds = \sqrt{x'(t)^2 + y'(t)^2}\ dt \tag{4}$$

where x' and y' are partial derivatives of t, and $n_1,\ n_2$ are real numbers from -1∼1. Finally, the second area moment for the hollow circular cross-section I_x is expressed as shown in (5).

$$I_x = \frac{rh^3}{12\pi}\int_{n_1}^{n_2}(-\pi sin\pi t)^2 dt + r^3h^3\int_{n_1}^{n_2}\pi\sin^2\pi t dt \tag{5}$$

To derive the second area moment for multilayer cylindrical structures, the radius r, and thickness h are expressed as follows in (5).

$$r = \frac{D-h}{2} \tag{6}$$

$$h = \ t \times m \tag{7}$$

Where D is the circular outside diameter, t is the paper thickness, and m is the number of layers.

Here, to derive the second area moment of the multilayer cylindrical structure, $n_1 = -1,\ \ n_2 = 1$ in (5), resulting in (8).

$$I_x = \frac{1}{12}\,\pi h^3 r + \pi h r^3 \tag{8}$$

Using (6) and (7), (8) is expressed by (9).

$$I_x = \frac{1}{24}\,\pi(tm)^3\,(D - tm) + \frac{1}{8}\pi tm(D - tm)^3 \tag{9}$$

III. Experimental Methods

A. Bistable Structure

Fig. 6(a) shows the design pattern of the bistable structure. The angle p_θ between adjacent printed lines was set to 45°. The hole was made in the center because overlapping printed lines would concentrate stress and prevent the desired fold from forming. The variable design parameters were the paper thickness t and the printed line width p_w. Table I shows the parameters of the three bistable structures used as samples. Different paper thicknesses t (67.9, 75.7, 80.5, 89.2, 97.3, 116, 131 μm) were used for the structures (a)–(c).

We conducted compression tests on the bistable structures and evaluated the force-displacement characteristics. The load and displacement required for state change were determined and fed back to the gripper design. Fig. 6(b) shows the experimental system of the compression test. The test system consists of a

TABLE I
DESIGN PARAMETERS OF BISTABLE STRUCTURE

		H	W	C_1	C_2	C_3	p_w	p_h
Length (mm)	(a)	100	100	10	29.03	10	10	50
	(b)	100	100	15	24.41	10	15	50
	(c)	100	100	20	19.79	10	20	50

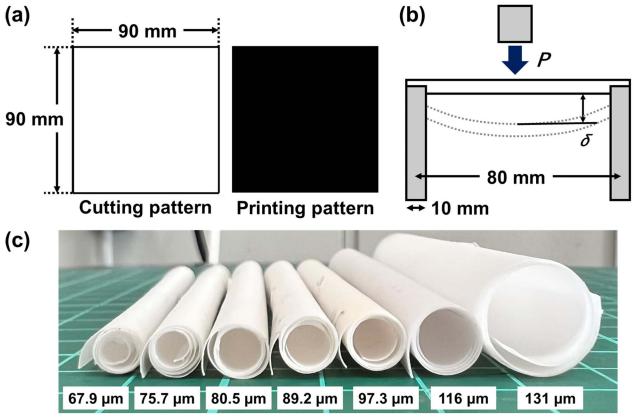

Fig. 7. Design and experimental setup of multilayer cylindrical structure. (a) Design. (b) Three point bending test. (c) Prototype.

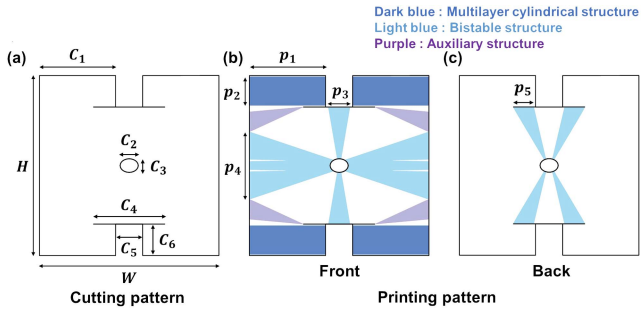

Fig. 8. Design of SOG. (a) Cutting pattern. (b) Front printing pattern. (c) Back printing pattern. Dark blue area corresponds to the multilayer cylindrical structure. Light blue area corresponds to the bistable structure. Purple area corresponds to realize the auxiliary structure.

TABLE II
DESIGN PARAMETERS OF SOG

(a) Cutting parameter

	H	W	C_1	C_2	C_3	C_4	C_5	C_6
Length (mm)	200	200	85	20	15	10	30	35

(b) Printing parameter

	p_1	p_2	p_3	p_4	p_5
Length (mm)	85	32	24	75	22.8

tensile and compression testing machine (MCT-1150, A&D), a compression fixture, and an installation substrate. The compression fixture and installation substrate were fabricated using a 3D printer. The compression fixture was installed on a load cell (LTS-50GAM2, KYOWA) rated at 500 mN. The compression fixture was installed to contact the top of the structure. Fig. 6(c) shows prototypes with varying print line width p_w. The wider the printing line width, the paper demonstrates larger folding angle, and highly bistable structures are formed. Three prototypes were fabricated and tested to verify reproducibility. The loading speed was 40 mm/min, and the sampling frequency was 10 Hz.

B. Multilayer Cylindrical Structure

Fig. 7(a) shows the printing pattern of the multilayer cylindrical structure. The structure can be fabricated by printing the solution on the entire surface. The variable design parameter is the paper thickness t. A three-point bending test was performed on the structure to confirm the rigidity improvement and verify the proposed analytical solution. Fig. 7(b) shows a schematic diagram of the experiment setup. The testing machine was the same as for the compression test, and the compression fixture was attached to the 500 N load cell (USM-500N, A&D). In this case, the installation platform and compression fixture were designed to apply the load to the center of the structure. The speed of the load was 20 mm/min, and the sampling interval was 20 μm.

The relationship between the load P and deflection δ in Fig. 7(b) is expressed as the following equation.

$$\delta = \frac{Pl^3}{48EI} \tag{10}$$

where l is the distance between the fulcrums, E is Young's modulus, and I is the second area moment, which can be obtained from (11).

$$I = \frac{Pl^3}{48\delta E} \tag{11}$$

Using I, the stiffness of the multilayer cylindrical structure can be evaluated. The distance between the fulcrums l was prepared as 80 mm, and Young's modulus of the paper E derived from the tensile test was 10.1 GPa.

As shown in Fig. 7(c), seven different structures were prepared with the different paper thickness. Using the results of the load-deflection curves obtained from the test, the stiffness k was calculated from the slope of the initial phase in the range from the starting point of the test to the peak. Finally, all obtained values were used to calculate the second area moment from (12).

$$I = \frac{Pl^3}{48\delta E} = \frac{kl^3}{48E} \tag{12}$$

Stiffness analysis was performed by comparing the proposed analytical solution of (9) with the values obtained from (12) and the experimental results.

C. Realization of SOG

Finally, the self-folded origami gripper (SOG) was realized by combining the bistable structure and the multilayer cylindrical structure. Fig. 8 shows the design pattern for SOG, and Table II shows the design parameters. In this study, we used an inkjet printer capable of printing up to A4-size, therefore we defined design parameters that could be produced from A4 paper. Since SOG requires mountain and valley folding, the printing pattern was defined on both sides. In Fig. 8, the printing pattern of bistable structure for switching is shown in the light blue area. the multilayer cylindrical structure to enhance the finger stiffness is shown in the dark blue area. The purple area of the printed

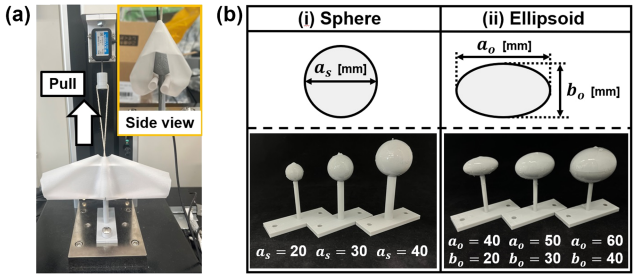

Fig. 9. Experimental setup for evaluation of grasping force. (a) Grasping test. (b) Grasping object.

pattern is added for the fingers to contact each other in grasping state. Fig. 3 and Movie S1 shows the automatic formation of the SOG.

D. Grasping Force Evaluation

We evaluated the grasping force to determine the optimal gripper design. The paper thickness of the gripper was selected at 116 μm. Fig. 9(a) shows the experimental system. The testing machine was the same as for the compression test. In the initial state, the gripper was set up to contact the finger part with the lower part of the object. As the tensile test proceeds, the gripper begins to move upward. We measured the force until the gripper peeled off from the object. The tensile speed was 40 mm/min, and the sampling frequency was 10 Hz. Three grippers were tested with printing line widths $p_4 = 45$, 60, 75 mm. Fig. 9(b) shows the grasping objects for the tensile test. The sphere and the ellipsoid shapes were prepared. The object was made by the 3D printer, and a thin layer of silicon was coated to give the object frictional force. The sphere-shaped objects had diameters of $a_s = 20$, 30, 40 mm, and the ellipsoid-shaped objects had diameters of $a_o = 40$, 50, 60 mm, while the short diameters were $b_o = 20$, 30, 40 mm.

IV. Results and Discussions

A. Bistable Structure

Fig. 10 shows the results of compression tests on the bistable structure. The test results obtained for the three samples were averaged. Fig. 10(a) summarizes the maximum load required for deformation. The maximum load increased as the paper became thicker. Also, for all paper thicknesses, the load increased with the wider printing line. When p_w is wide, the area of the paper that reacts with the printed solution is large. The reacted part makes the structure stiffer. Moreover, the larger folding angle increases rigidity of the structure with increasing the second area moment. Therefore, the maximum load increased. The structure with the highest load was the one with a paper thickness of $t = 116$ μm and a print line width $p_w = 20$ mm, with a load of 0.33 N. This load was 550% of the structure with the lowest load, $t = 67.9$ μm and $p_w = 10$ mm.

Next, Fig. 10(b) summarizes the displacement required for deformation. The wider p_w showed the larger displacement. As discussed in the load experiment, when p_w is wide, a large hinge is formed to present large folding angle. The height of the final structure became higher, and the displacement required to deform ($S_0 - S_1$ in Fig. 4(b)) increased. The displacement tended

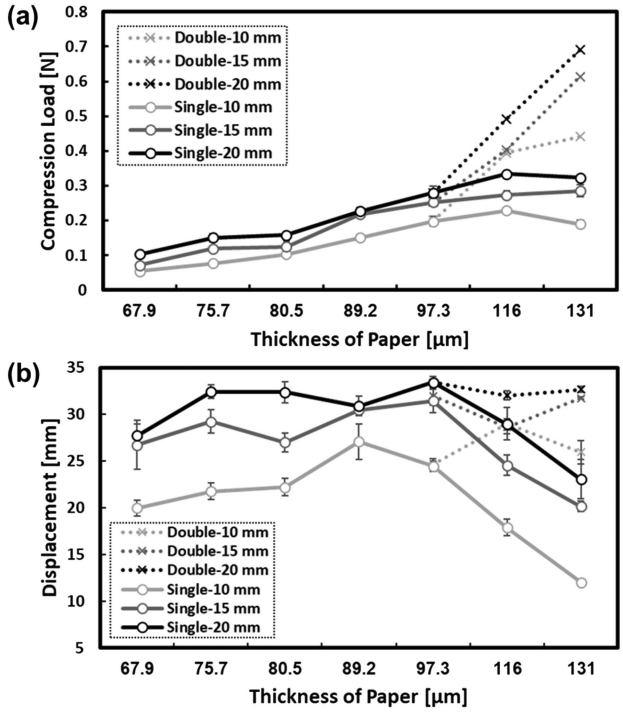

Fig. 10. Results of compression tests for bistable structure. Required (a) loads and (b) displacements for transitioning from the open state to the closed state. The thicker the paper, the greater the force required for transit. The performance of the gripper made from the thick paper improves by increasing the coating amount through overprinting.

to increase to the structure with $t = 97.3$ μm. However, when the paper is thicker than 116 μm, the displacement decreased. This is because the amount of ink applied was insufficient. The ink did not spread in the direction of the paper thickness, which results in a lack of reaction volume. The compression test was performed on the bistable structure printed twice on the paper with the thicker papers ($t = 116$ and 131 μm). The results showed that the load and displacement increased rather than the single printed one. It was found that the right amount of solution printing was needed to improve mechanical properties on thicker paper. The relationship between paper thickness and ink penetration is discussed in detail in the next chapter. The structure with the most significant displacement was the one with $t = 97.3$ μm and $p_w = 20$ mm, with a displacement of 33.4 mm. This structure had 276% displacement of the structure with $t = 131$ μm and $p_w = 10$ mm, which had the smallest displacement. When the force and displacement required for deformation are small, minute external noise causes unexpected buckling. Thus, switching sensitivity can be controlled by varying paper thickness, printing line width, and ink application volume. Eventually, thickening the paper and widening p_w is important to develop the stable gripper, which deforms at the desired timing.

B. Multilayer Cylindrical Structure

Fig. 11 shows the results of a three-point bending test on the multilayer cylindrical structure. First, we investigated the effect of paper thickness on the shape of the multilayer cylindrical structure. Fig. 11(a) shows the results of the number of layers and the outer diameter of the multilayer cylindrical structure

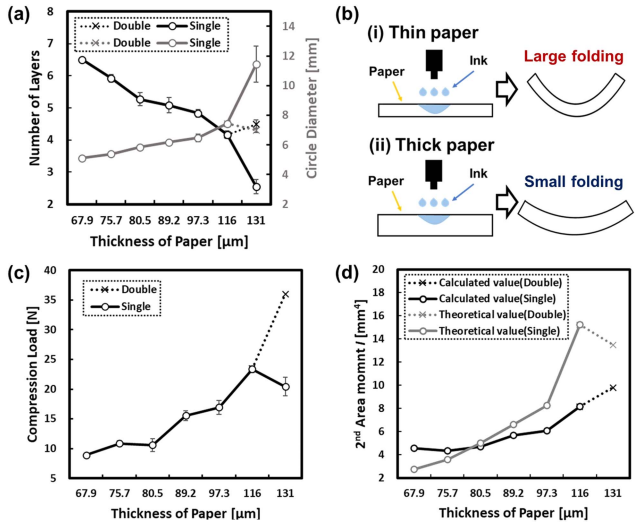

Fig. 11. Experimental results of multilayer cylindrical structure. (a) Relationship between the number of layers and circular diameter against paper thickness. (b) Difference in deformation due to ink penetration and paper thickness. (c) Relationship between paper thickness and compression load obtained from three-point bending test. (d) Relationship between theoretical and calculated values of second area moment against paper thickness.

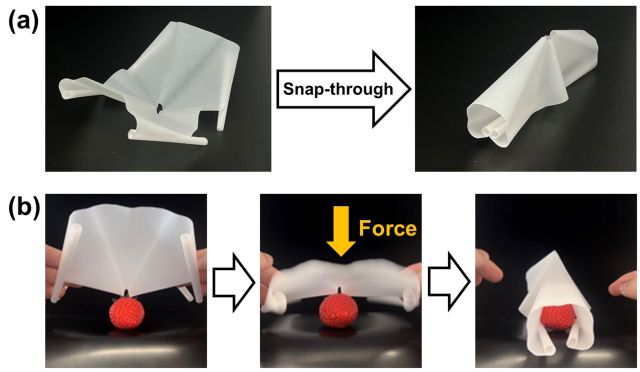

Fig. 12. Demonstration of SOG. (a) Bistability of gripper. (b) Grasping process.

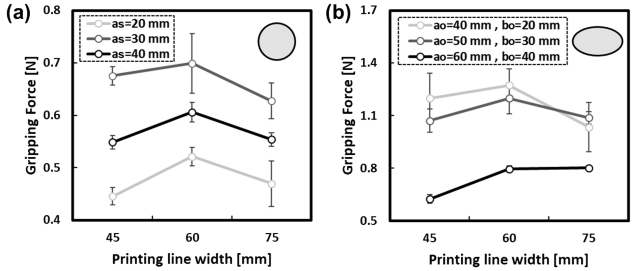

Fig. 13. Results of grasping force evaluation. (a) Sphere. (b) Ellipsoid.

as a function of paper thickness. The thicker the paper, the less the paper folded and the larger the outer diameter. Since the experiment was conducted with a constant paper size, the number of layers was reduced when the outer shape was large. This characteristic can be clearly observed as shown by the prototypes in Fig. 7(c). The structure with the highest paper thickness of $t = 131$ μm had 2.55 layers, while the thinnest paper thickness of $t = 67.9$ μm had 6.5 layers. The paper thickness also increased the circular outer diameter. The outer diameter was 5.12 mm at the thickest $t = 131$ μm and 11.4 mm at the thinnest $t = 67.9$ μm.

Fig. 11(b) shows the difference in folding magnitude by paper thickness. When the paper is thin, the ink penetrates the entire cross-section. The magnitude of folding becomes larger, since reaction between the solution increases. Therefore, the number of layers wound in a circular shape increase, and the outer diameter of the circular structure becomes smaller. Meanwhile, when the paper is thick, the ink penetrates only a part of the cross-section, which results in weaker reactivity and smaller bending. The number of layers became less due to the lack of ink penetration. At the same time, the outer diameter of the circular structure became larger. From the above, it is estimated that there is an optimum amount of ink to be applied depending on the paper thickness.

Fig. 11(c) shows the maximum load results for different paper thicknesses. The thicker the paper, the higher the load. The structure that withstood the maximum load was the structure with $t = 116$ μm. The maximum load was 23.5 N, indicating that this structure can withstand a load of approximately 2.4 kg. In the case of $t = 131$ μm, the load was smaller than that of the structure with $t = 116$ μm when printed once. However, the thick papers were folded significantly by printing twice, and the structure that could withstand a more significant load could be realized. When printed twice, the load was 176% higher than the structure which was printed once.

Fig. 11(d) shows the comparison of the second area moment based on our proposed theoretical equation and the calculated value obtained from the experimental data. The theoretical and calculated values show the same trend, and the second area moment increased as the paper thickness increased. The proposed equation allows us to estimate the stiffer cylindrical structure. The cause of the error between theoretical and experimental values is due to the flexibility of the paper. The flexibility of the paper itself causes deformation from the top of the structure during compression. The paper does not deform in the hollow circle structure as in the theoretical equation, which is thought to be the reason for the decrement from the theoretical values to the calculated values.

Equation (9) is valid when $D \gg tm$, and monotonically increasing for both D and m. Since the paper size was constant for the experiment, there was a trade-off between the outer diameter D and the number of layers m. The cylindrical structure with thicker paper, which showed larger D and less m, presented higher rigidity, because D is more dominant in (9). The gripper with stiff fingers can grasp heavier objects. However, it is difficult to grasp a small or thin object with the larger finger. Therefore, the experimental result suggests that it is necessary to change the finger design depending on the shape and weight of the object. The derived analytical solution allows the calculation of the second area moment of the cylindrical structure to induce the optimal design of the gripper.

C. Realization of SOG

The compression test results of the bistable structure showed that the load required for snap-through increased as the printing line width p_w increased, however all the values were smaller than

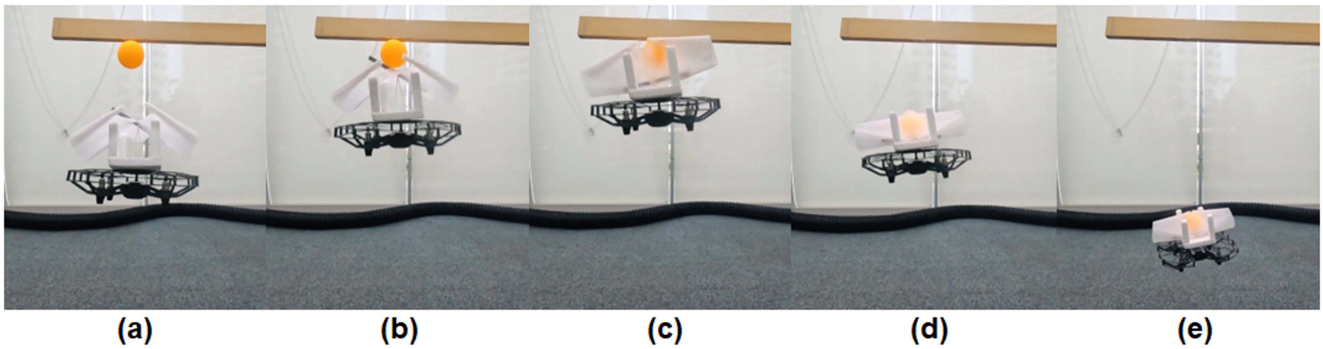

Fig. 14. Grasping experiment equipped with a quadcopter. (a) Ascent process to the object. (b) Contact to the object to grasp. (c) Initiation of grip through contact-trigger activation. (d)–(e) Descent towards the destination.

500 mN. The thrust of the quadcopter (Ryze Tech Tello, DJI) employed in the demonstration was measured using a load cell (LTS-500GAM2, KYOWA), and the value was approximately 700 mN. The quadcopter can fly while mounting the SOG, and the SOG is sufficiently capable of being controlled open-close switching by the thrust power. The bending test results of the multilayer cylindrical structure showed that the structure with the paper thickness of $t = 116$ µm had the best load-bearing capacity. Therefore, the paper with the thickness of $t = 116$ µm was employed for the SOG.

Fig. 12 shows the developed SOG. As shown in Fig. 12(a), the bistable structure has two states, one with the open state and the other with the closed state. Fig. 12(b) shows the grasping process. Initially, the gripper is the open state. When the center of the gripper is contacted with an object, the force is applied to the protrusion, and it changes to a closed state. Even after deformation to the closed structure, no additional energy is required to maintain the structure. Therefore, the grasping can be achieved only by contact with the object. The demonstrations are also shown in the Supporting Information Movies S2 and S3.

D. Grasping Force Evaluation

Fig. 13 shows the results of the grasping experiments. Fig. 13(a) shows the results of the grasping experiment for the sphere object. The results show that the sphere size suitable for grasping is $a_s = 30$ mm. The printing line width of the gripper with the highest grasping force performance tended to be $p_4 = 60$ mm. The highest grasping force was 0.68 N at $a_s = 30$ mm and $p_4 = 60$ mm. This was about 151% higher than the lowest grasping force of $a_s = 20$ mm, $p_4 = 45$ mm.

Fig. 13(b) shows the results of the grasping experiment for the ellipsoid object. From the results, we found that $a_o = 40$ mm and $b_o = 20$ mm is the most suitable ellipsoid size for grasping. In addition, the printing line width of the gripper with high grasping force performance tended to be $p_4 = 60$ mm, which is the same as that of the sphere. The highest grasping force was 1.27 N at $a_o = 40$ mm, $b_o = 20$ mm, and $p_4 = 60$ mm. This was about 205% more than the lowest grasping force of $a_o = 60$ mm, $b_o = 40$ mm and $p_4 = 45$ mm.

These differences of the grasping performance are primarily related to the finger's position relative to the object and the degree of finger opening. The closer the surface of the object in contact with the finger is to the horizontal, the larger the grasping force is obtained. When the finger opens larger, the elastic hinge is deformed to be wider than the initial state. Since the elastic restoring force increases due to the large deformation, the grasping force increases. Regarding the printing line width p_4, the self-folding technology is characterized by an increase in foldability when the printing line width is wide and printed in the direction of the paper fiber. In the case of $p_4 = 45$ mm, the isosceles triangle in the printed pattern does not change its inclination much in the fiber direction, however p_4 being small. On the other hand, in the case of $p_4 = 75$ mm, the printing line width is wider, however the isosceles triangles of the printing patterns have a significant inclination for the fiber direction. Therefore, $p_4 = 60$ mm, which compensates for these disadvantages, is considered to have generated the larger grasping force.

We also compared the grasping performance between the hand-folded gripper and SOG. In the case of a sphere ($a_s = 30$ mm), the grasping force of the hand-folded gripper was about 0.26 N. On the other hand, the SOG had a grasping force of 0.68 N, which is approximately 2.62 times greater. We confirmed that the elastic memory characteristics of the self-folding technology improves the grasping performance. The paper properties imparted by the self-folding technology are critical to the performance of the SOG.

V. Flying Demonstration

We mounted the developed SOG on the quadcopter (Ryze Tech Tello, DJI) and attempted to grasp an object. Fig. 1 shows the quadcopter mounted with the SOG. We attached a fixation material made of styrene foam to the top of the quadcopter. The fixation material supports the SOG with four legs, suppressing the SOG wobble that occurs when the quadcopter is in flight. Furthermore, the fixation material facilitates the deformation of the SOG when the SOG is in contact with an object. During experiments of object grasping, the SOG is connected to the fixation material via the rod and thread installed inside the gripper. We chose a low-cost and compact quadcopter to demonstrate the lightweight and compactness of the SOG. We also confirmed in advance that higher flight stability is achieved when the SOG was mounted at the top of the quadcopter rather than at the bottom. In addition, no trigger malfunctions occurred when the quadcopter moved sideways at the maximum speed of 8 m/s.

Fig. 14 and Movie S4 show the demonstration result of the object grasping while flying. First, as shown in Fig. 14(a), the SOG was attached to the quadcopter in an open position and approached the object. Then, as shown in Fig. 14(b), the

quadcopter contacts the object, and a trigger force is applied to the SOG. This trigger force causes the gripper to shift to a closed structure according to the bistable mechanism, as shown in Fig. 14(c). As shown in Fig. 14(d), the SOG has achieved the grasping of a spherical object. Finally, as Fig. 14(e) shows, the quadcopter left with the object grasped. Thus, the bistable mechanism fabricated using the paper self-folding technology has successfully developed an origami soft gripper that can be mounted on an inexpensive quadcopter.

VI. Conclusion

In this letter, we developed the Self-folded Origami Gripper (SOG), based on origami technology. SOG can be fabricated using self-folding technology based on inkjet printing and can autonomously add elastic memory characteristics and rigidity to a sheet of paper. By utilizing these properties and incorporating a bistable structure and multilayer cylindrical structure into the folded paper structure of the SOG, we have achieved a simple control that allows grasping only by contact with the object. Finally, we successfully mounted SOG on the inexpensive and low-payload quadcopter for object grasping by contact.

The proposed SOG is made of paper and inherits biodegradability. It is also lightweight and strong due to the employment of origami technology. As a result, it can fly stably with low cost and low power consumption and is expected to be used as a new green device with providing additional function for quadcopter applications. The SOG proposed in this paper will be the basis for future intelligent origami devices to provide a quadcopter multifunction.

Acknowledgment

The authors would like to thank V. Cacucciolo for discussions about theoretical equation.

References

[1] J. Shintake, V. Cacucciolo, D. Floreano, and H. Shea, "Soft robotic grippers," *Adv. Mater.*, vol. 30, no. 29, 2018, Art. no. 1707035.
[2] Y. Cui, X.-J. Liu, X. Dong, J. Zhou, and H. Zhao, "Enhancing the universality of a pneumatic gripper via continuously adjustable initial grasp postures," *IEEE Trans. Robot.*, vol. 37, no. 5, pp. 1604–1618, Oct. 2021.
[3] J. Shintake, S. Rosset, B. Schubert, D. Floreano, and H. Shea, "Versatile soft grippers with intrinsic electroadhesion based on multifunctional polymer actuators," *Adv. Mater.*, vol. 28, no. 2, pp. 231–238, 2016.
[4] Y. Yang, K. Vella, and D. P. Holmes, "Grasping with kirigami shells," *Sci. Robot.*, vol. 6, no. 54, 2021, Art. no. eabd6426.
[5] L. Li et al., "Aerial-aquatic robots capable of crossing the air-water boundary and hitchhiking on surfaces," *Sci. Robot.*, vol. 7, no. 66, 2022, Art. no. eabm6695.
[6] C. Geckeler and S. Mintchev, "Bistable helical origami gripper for sensor placement on branches," *Adv. Intell. Syst.*, vol. 4, no. 10, 2022, Art. no. 2200087.
[7] W. R. Roderick, M. R. Cutkosky, and D. Lentink, "Bird-inspired dynamic grasping and perching in arboreal environments," *Sci. Robot.*, vol. 6, no. 61, 2021, Art. no. eabj7562.
[8] L. Y. Lee, O. A. Syadiqeen, C. P. Tan, and S. G. Nurzaman, "Closed-structure compliant gripper with morphologically optimized multi-material fingertips for aerial grasping," *IEEE Robot. Automat. Lett.*, vol. 6, no. 2, pp. 887–894, Apr. 2021.
[9] H. Zhang, E. Lerner, B. Cheng, and J. Zhao, "Compliant bistable grippers enable passive perching for micro aerial vehicles," *IEEE/ASME Trans. Mechatron.*, vol. 26, no. 5, pp. 2316–2326, Oct. 2021.
[10] S. A. Zirbel et al., "Accommodating thickness in origami-based deployable arrays," *J. Mech. Des.*, vol. 135, no. 11, 2013, Art. no. 111005.
[11] A. P. Thrall and C. P. Quaglia, "Accordion shelters: A historical review of origami-like deployable shelters developed by the US military," *Eng. Struct.*, vol. 59, pp. 686–692, 2014.
[12] S. Li et al., "A vacuum-driven origami 'magic-ball' soft gripper," in *Proc. Int. Conf. Robot. Automat.*, 2019, pp. 7401–7408.
[13] S. Felton, M. Tolley, E. Demaine, D. Rus, and R. Wood, "A method for building self-folding machines," *Science*, vol. 345, no. 6197, pp. 644–646, 2014.
[14] T. G. Nelson, R. J. Lang, S. P. Magleby, and L. L. Howell, "Curved-folding-inspired deployable compliant rolling-contact element (D-CORE)," *Mechanism Mach. Theory*, vol. 96, pp. 225–238, 2016.
[15] S. J. Kim, D. Y. Lee, G. P. Jung, and K. J. Cho, "An origami-inspired, self-locking robotic arm that can be folded flat," *Sci. Robot.*, vol. 3, no. 16, 2018, Art. no. eaar2915.
[16] P. Sareh, P. Chermprayong, M. Emmanuelli, H. Nadeem, and M. Kovac, "Rotorigami: A rotary origami protective system for robotic rotorcraft," *Sci. Robot.*, vol. 3, no. 22, 2018, Art. no. eaah5228.
[17] S. Mintchev, J. Shintake, and D. Floreano, "Bioinspired dual-stiffness origami," *Sci. Robot.*, vol. 3, no. 20, 2018, Art. no. eaau0275.
[18] E. A. Peraza-Hernandez, D. J. Hartl, R. J. Malak Jr, and D. C. Lagoudas, "Origami-inspired active structures: A synthesis and review," *Smart Mater. Struct.*, vol. 23, no. 9, 2014, Art. no. 094001.
[19] E. A. Peraza-Hernandez, D. J. Hartl, and R. J. Malak Jr., "Design and numerical analysis of an SMA mesh-based self-folding sheet," *Smart Mater. Struct.*, vol. 22, no. 9, 2013, Art. no. 094008.
[20] Q. Ge, A. H. Sakhaei, H. Lee, C. K. Dunn, N. X. Fang, and M. L. Dunn, "Multimaterial 4D printing with tailorable shape memory polymers," *Sci. Rep.*, vol. 6, no. 1, pp. 1–11, 2016.
[21] H. Shigemune, S. Maeda, Y. Hara, N. Hosoya, and S. Hashimoto, "Origami robot: A self-folding paper robot with an electrothermal actuator created by printing," *IEEE/ASME Trans. Mechatron.*, vol. 21, no. 6, pp. 2746–2754, Dec. 2016.
[22] H. Shigemune et al., "Printed paper robot driven by electrostatic actuator," *IEEE Robot. Automat. Lett.*, vol. 2, no. 2, pp. 1001–1007, Apr. 2017.
[23] B. H. Hanna, J. M. Lund, R. J. Lang, S. P. Magleby, and L. L. Howell, "Waterbomb base: A symmetric single-vertex bistable origami mechanism," *Smart Mater. Struct.*, vol. 23, no. 9, 2014, Art. no. 094009.
[24] H. Han, L. Tang, D. Cao, and L. Liu, "Modeling and analysis of dynamic characteristics of multi-stable waterbomb origami base," *Nonlinear Dyn.*, vol. 102, no. 4, pp. 2339–2362, 2020.
[25] Y. Fukatsu and H. Shigemune, "Development of self-folded corrugated structures using automatic origami technique by inkjet printing," *Adv. Intell. Syst.*, vol. 4, 2022, Art. no. 2100260.